Theoretical Investigation of the Structural Properties of Two Crotamines Isolated from the Venom of *Crotalus durissus*

Antônio Flávio de C. Alcântara*[,1], Dorila Piló-Veloso[1], Antônio José do N. Fernandes[2] and Maria C. Dos-Santos[2]

[1]*Departamento de Química, ICEx, Universidade Federal de Minas Gerais, 31160-901, Belo Horizonte – MG, Brazil*

[2]*Departamento de Parasitologia, Instituto de Ciências Biológicas, Universidade Federal do Amazonas, 69077-000, Manaus – AM, Brazil*

Abstract: Crotamines **1** and **2** differ only at residue 19 (which is Leu in **1**, and Ile in **2**), but **1** presents a greater myonecrotic activity. PM3 geometry optimizations of fragments of **1** (I17-C18-L19-P20-P21) and **2** (I17-C18-I19-P20-P21) yielded the minimum energy conformations **I-a** and **II-a**, respectively. The HF and DFT calculation of chemical properties (atomic charge, orbital population, and MO energy) of **I-a** and **II-a** did not reveal significant differences that would explain the differences in biological activities of the corresponding crotamines. PM3 optimized geometries of full peptides **1** and **2** presented different globular spatial arrangements when disulfide bonds between cysteine residues were considered. This fact may be related to the difference in biological activities observed for the two crotamines.

Keywords: Crotamines, myonecrotic activity, conformational analysis of peptides, theoretical calculations.

1. INTRODUCTION

Crotamine **1** is a peptide with 42 amino acid residues [1] (Scheme **1**) that is widely distributed among the *Crotalus* snake venoms [2] and is characterized as a cell-penetrating neurotoxin [3] which induces persistent activation of the sodium channel [4], inhibits the direct transition of channels from closed to inactivated states, thereby forcing their transition through the open states [5], shows analgesic activity [6], and is myonecrotic [7, 8]. Crotamine **2** shows a high degree of homology with **1**, differing only by having an isoleucine residue in position 19 instead of leucine.

Some differences in the biological activities of these two crotamines have previously been observed [9]. For example, intramuscular injection of **1** in mice induces immediate hyperextension in the affected paw with subsequent hind limb paralysis, ptosis, lachrymal hypersecrection, dyspnea, tachycardia, and absence of response to mechanical stimuli 20 min after injection. Total limb paralysis, tachycardia, dyspnea, and pronounced ptosis occur and last for 24 h. In addition, the histological study of the gastrocnemius muscle revealed intense cytoplasm vacuolization on 24 h after injection of **1**. Similarly, hyperextension of the injected paw with subsequent hind limb paralysis, ptosis, and tachycardia are observed when **2** is injected under the same experimental conditions. However, all signals and symptoms disappear only within 30 min after the injection. Moreover, no lesions are observed when **2** is injected to mice.

The differences in the biological activities of these crotamines should be arisen from the alteration in residue 19 [8]. Therefore, the question is whether the intrinsic chemical properties of leucine and isoleucine can explain the more active myonecrotic site of **1**, or whether the different steric influences of residue 19 simply alter the overall three-dimensional structure of these crotamines so as to alter the geometry and, hence, the myonecrotic activity in the target cell. To answer these questions, it would be appropriate to investigate the electronic and structural properties of crotamines **1** and **2**.

Conformation simulations of crotamine **1** based on NMR and CD data have previously been published [10, 11]. A conformational study was also performed by theoretical calculations using the molecular mechanics method (MM) [13]. In both these cases, the globular conformations of **1** were obtained. In the present work, theoretical investigation of the chemical and structural properties of these crotamines was carried out to relating to their myonecrotic activities. The chemical and structural properties of fragments that include residue 19 of **1** and **2** were investigated using the Hartree-Fock (HF) and the Density Functional Theory (DFT) theoretical calculations. Additionally, the conformational analysis by semi-empirical PM3 calculations was also performed to investigate the stereochemistry effects of residue 19 on the myonecrotic activity of these crotamines.

2. COMPUTATIONAL METHODS

Theoretical studies were accumplished using the GAUSSIAN03 software package [13]. Geometry optimizations were performed using the semi-empirical PM3 method [14]. The Hartree-Fock method [15] was employed using a 6-31G* basis set (HF/6-31G*) [16, 17]. The Density Functional Theory method [18] utilized the BLYP and B3LYP [19, 20] functions in the same basis set (BLYP/6-31G* and B3LYP/6-31G*, respectively). DFT methods have been very popular for the calculations of larger molecules such as bio-

*Address correspondence to this author at the Departamento de Química, ICEx, Universidade Federal de Minas Gerais, 31160-901, Belo Horizonte – MG, Brazil; Tel: +553134095728; Fax: +553134095700;
E-mail: aalcantara@zeus.qui.ufmg.br

1874-8481/11

Y1-K2-Q3-C4-H5-K6-K7-G8-G9-H10-C11-F11-P13-K14-E15-K16-I17-C18-**L19**-P20-P21-S22-S23-D24-F25-G26-K27-M28-D29-C30-R31-W32-P33-W34-K35-C36-C37-K38-K39-G40-S41-G42

Scheme 1. Alignment of crotamine **1** in one-letter amino acid code.

molecules. In many cases, the results of DFT calculations agree quite satisfactorily with experimental data. The HF method does not include coulombic electron-electron repulsion in the calculation. However, its net effect is included in the calculation. DFT methods compute electron correlations and achieve significantly greater accuracy than HF theory. However, the DFT methods demand more computational resources, being more expensive than an equivalent Hartree-Fock calculation. Since the quality of the results depends critically on the function for DFT calculations, the pure (BLYP) and hybrid (B3LYP) DFT methods were used in the theoretical investigations of the crotamines. The hybrid B3LYP function can be considered to be superior to the pure function BLYP, but also demands greater computational resources [21, 22].

HF/6-31G* and BLYP/6-31G* geometry optimizations were performed for structures in the gaseous phase. The solvent effect was approximated by the Polarizable Continuum Model (PCM) as implemented in the Gaussian03 package for optimized geometries at the B3LYP/6-31G* level with water (ε = 78.4) as the solvent [B3LYP/6-31G* (PCM; water)] [23]. All the structures obtained from theoretical calculations were characterized as true energy minima on the Potential Energy Surfice (PES) through frequency calculations (when the frequencies are real, a true minimum energy structure is present).

Conformational analysis by PM3 calculations on fragments I17-C18-L19-P20-P21 (**I**) and I17-C18-I19-P20-P21 (**II**) were performed for structures with non-ionized termini in the gaseous phase. The optimized geometries were re-optimized at the HF/6-31G*, BLYP/6-31G*, and B3LYP/6-31G* (PCM; water) levels. The atomic charge properties (Mulliken), the orbital populations, and the molecular orbital (MO) energies of these fragments were obtained at the same levels of theory. These chemical properties have efficiently calculated for several organic compounds [24-26].

Conformational analyses of **1** and **2** were accomplished for PM3 calculations by stepwise additions of amino acid residues and geometry optimizations based on the geometries of fragments **I** and **II,** optimized by B3LYP/6-31G*(PCM; water) [27, 28]. In this manner, S22 was added to the *C*-terminal of both fragments following geometry optimizations of these new six-residue fragments. The K16 was then added to the *N*-terminal of these most recent fragments containing seven residues, and geometry optimizations were again performed. The addition of residues to either the *C*-terminal or the *N*-terminal residue, followed by geometry optimization, was performed successively until the optimizations of the complete sequences of **1** and **2** were achieved. In all these cases, the calculations were performed for structures with ionized termini in the gaseous phase.

3. RESULTS AND DISCUSSION

Theoretical Calculations of the Fragments

Conformational investigation of fragment **I** was initially performed by PM3 geometry optimizations. From the 11 optimized geometries (**I-a** to **I-k**), conformation **I-a** presented the lowest enthalpy (ΔH_f = -234.56 kcal/mol). All the other conformations, **I-b** to **I-k**, presented enthalpies higher than ΔH_f = -231.69 kcal/mol. Likewise, geometries corresponding to fragment **II** were generated from **I-a** to **I-k** by replacing Leu by Ile at position 19. PM3 geometry optimizations resulted in two conformations having similar enthalpies, lower than all the others, namely **II-a** (ΔH_f = -231.99 kcal/mol) and **II-b** (ΔH_f = -231.09 kcal/mol). The other conformations, **II-c** to **II-k**, had ΔH_f > -229.28 kcal/mol. Since **II-a** and **II-b** presented similar geometries, only **II-a** will be considered henceforth.

HF/6-31G*, BLYP/6-31G*, and B3LYP/6-31G*(PCM; water) Mulliken atomic charge calculations for all the atoms of **I-a** and **II-a** were also performed for structures with non-ionized termini. The atomic charge relationships obtained between corresponding atoms of **I-a** and **II-a** did not show significant differences. As a result of these relationships, atomic charges certainly do not constitute a determining parameter that might be related to the potential myonecrotic activity observed for **1** and **2**. HF/6-31G*, BLYP/6-31G*, and B3LYP/6-31G*(PCM; water) calculations of orbital populations, as well as occupied and vacant MO energies, for **I-a** and **II-a** were performed for structures with non-ionized terminal residues. A comparison of the orbital population and MO energies did not reveal significant differences. It follows that both properties of these fragments do not determine the biological activities of the corresponding crotamines.

Fig. (**1**) shows the conformations **I-a** and **II-a** obtained from B3LYP/6-31G*(PCM; water)-geometry optimizations for structures with non-ionized termini. The spatial arrangements of the PM3, HF/6-31G*, and BLYP/6-31G* optimized geometries of **I-a** and **II-a** are almost the same as those obtained for the B3LYP/6-31G*(PCM; water) geometry optimizations. All the geometry optimizations of **I-a** and **II-a** place the carbonyl oxygen of P20 (O–P20) close to amide hydrogen of C18 (H–C18). The interatomic distances observed in all these calculations are lower for **II-a** than for **I-a**, indicating a steric effect for residue 19 of **II-a** that favors a stronger hydrogen bond between the O–P20 and the H–C18. As a consequence, **II-a** presents a more pronounced folding near residue 19 than the corresponding region of **I-a**. Another consequence of these results is some loss of well-defined secondary structures (helicoidal or β-sheet forms) near I19 of **II-a**, schematically shown in Fig. (**1**) by the break in the ribbon chain (tape) of this fragment. The O–P20 and H–C18 intramolecular interactions exist to maintain stability and also probably aid in the folding of the main chain, and may have consequences for the large-scale conformation of these crotamines [29]. Thus, since most of the calculated differences in the O–P20 and the H–C18 interatomic distances for **I-a** and **II-a** may not be significant, this fact may suggest an explanation based on differences in the spatial arrangements of the terminal residues of both crotamines.

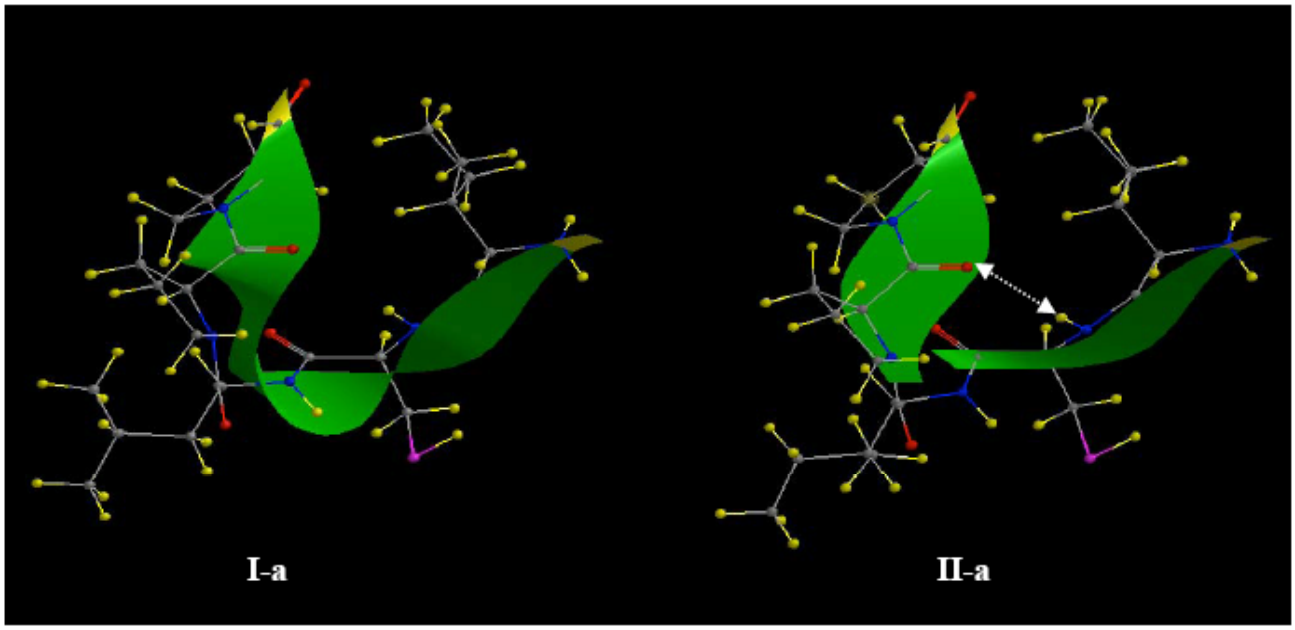

Fig. (1). B3LYP/6-31G* optimized geometries of **I-a** and **II-a**, for structures with non-ionized termini in the gaseous phase. The double arrow shows the proximity between the carbonyl oxygen of residue P20 and the hydrogen of the amine group of residue C18.

Geometry Optimizations of the Crotamines 1 and 2

By beginning with the geometries of **I-a** and **II-a** optimized by B3LYP/6-31G*(PCM; water) calculations, PM3 geometry optimizations of larger fragments of **1** and **2** were calculated for structures with ionized termini, in the gaseous phase, without considering intramolecular disulfide bonds between cysteine residues. The new fragments were constructed by alternate stepwise additions of the respective residues to the *N*-terminal and the *C*-terminal residues to complete the full sequences, followed by the corresponding conformational analyses of both crotamines. The geometries were optimized after each addition.

The resulting conformation analysis of **1** demonstrated a globular spatial arrangement at the *N*-terminal end, i.e. from Y1 to K16. In the region between K16 and P21, including L19, there is a relatively linear substructure. From F25 to M28, P33 to S41, and at the *C*-terminal residue, a somewhat helicoidal form is apparent. The fully-characterized helicoidal form between P33 and S41 has already been related to the disulfide bonds involving the cysteine residues in positions 36 and 37 [30]. The infrequent occurrence of helices in the PM3-optimized geometry of **1** agrees with the *ca*. 2% of this form predicted by circular dichroism analysis [10, 11, 31].

The optimized geometry of **2** is more linear than **1**, except for a pronounced inflexion between I19 and P21 in **2**. At the *N*-terminal residue, there is a pronounced inflexion of the coil between K7 and H10. Nevertheless, the conformational differences were observed in the spatial arrangement at the chain termini of these crotamines. Since experimental studies revealed that fragments containing residues at the terminus of **1** show myonecrotic activity [1, 32], the different spatial arrangements at the ends of these crotamines could be related to the differences in the biological activities.

Theoretical calculations were performed for both crotamines with structures containing the three disulfide bonds between C4–C36, C11–C30, and C18–C37, as proposed earlier [12]. The PM3 optimized geometries of **1** and **2** were used as starting models. Since the structures of these crotamines without disulfide bonds are different, they could lead to distinct sequences of disulfide bond formation, so PM3 theoretical calculations were performed for conformational analyses of these crotamines with different sequences for disulfide bond formation. A C4–C36 disulfide bond was formed, followed by further geometry optimizations by the additions of the C11–C30 and C18–C37 links, successively, giving the structures shown in Fig. (**2a**) for both crotamines.

The optimized geometries of **1** and **2** were obtained from the C11–C30, C18–C37, and C4–C36, as well as from the C18–C37, C4–C36, and C11–C30 sequences of disulfide bond formation, respectively shown in Fig. (**2b** and **2c**). Hence, different optimized geometries can be observed when the sequences of disulfide bond formation are changed. Among the geometries of these crotamines shown in Fig. (**2a-2c**), the lowest energies correspond to **1(a)** and **2(c)**, respectively. Although these conformations are all globular, they probably differ in their intermolecular interactions. The disulfide bond formation between C4–C37, C11–C36, and C18–C30 was also considered, as was previously proposed for some crotamines [33]. Similar results were obtained with different optimized geometries when the sequences of the disulfide bond formation were changed.

CONCLUSION

Although both crotamines have a high degree of homology, **1** shows greater myonecrotic activity than **2**. In light of this result, PM3, HF/6-31G*, BLYP/6-31G*, and B3LYP/6-31G*(PCM; water) calculations were used to obtain data with regard to the chemical properties of the fragments of both crotamines. Even though there are some variations in the chemical properties between both fragments, no rigorous

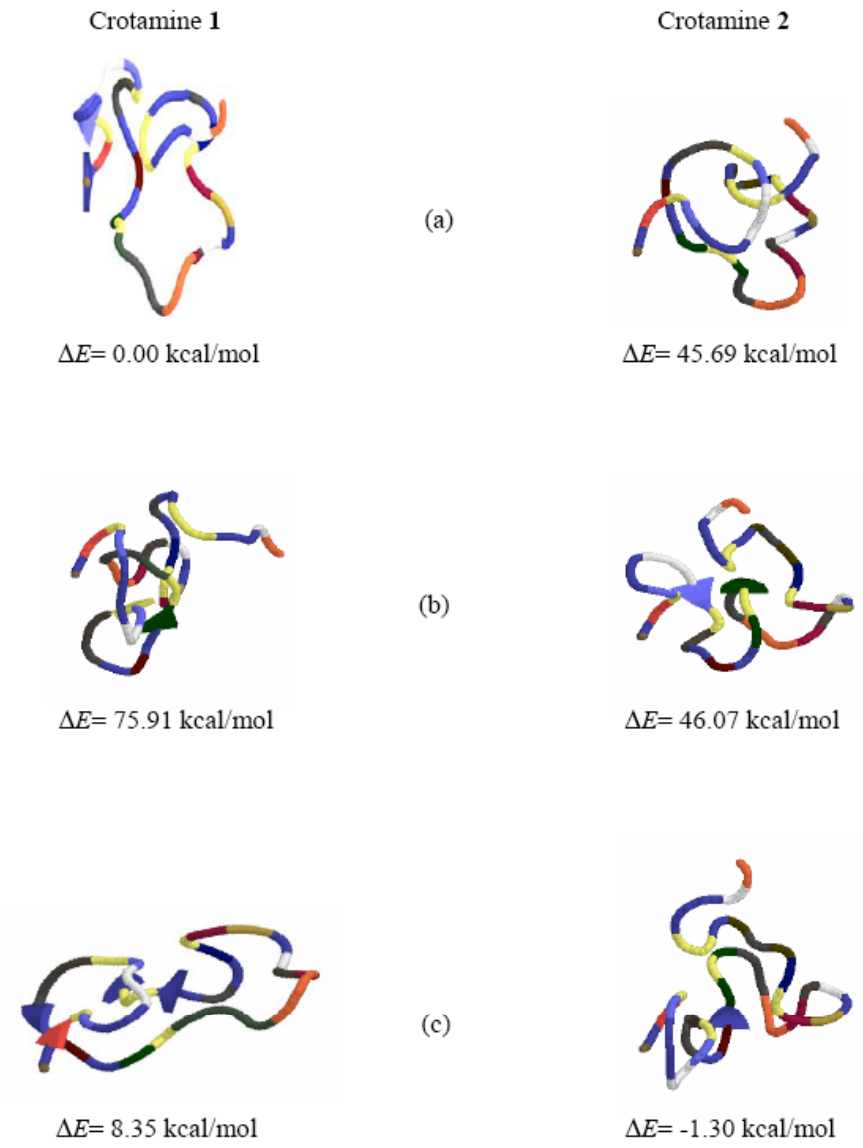

Fig. (2). PM3-optimized geometry of **1** and **2** with ionized termini in the gaseous phase, performed by stepwise formation of disulfide bonds in accord with the sequences: (**a**) C4–C36, C11–C30, and C18–C37, (**b**) C11–C30, C18–C37, and C4–C36, and (**c**) C18–C37, C4–C36, and C11–C30. Energies relative to crotamine **1(a)**.

relationship to their respective biological activities can be established.

When disulfide bonds are not considered in the conformational analyses, the PM3 optimized geometry of **1** is less linear than that of **2**. Each conformation may favor specific intermolecular interactions and must play a determining role in defining their reactivities. As a result, different globular spatial arrangements can be proposed when alteration of the sequence of disulfide bond formation is considered for **1** and **2.** These arrangements are very likely to be related to the different conformations and activities observed for both crotamines.

ACKNOWLEDGEMENTS

The authors thank the Conselho Nacional de Desenvolvimento Científico e Tecnológico (CNPq), the Fundação Coordenação de Aperfeiçoamento de Pessoal de Nível Superior (CAPES), the Fundação de Amparo à Pesquisa do Estado de Minas Gerais (FAPEMIG), and the Fundação de Amparo à Pesquisa do Estado do Amazonas (FAPEAM). We are very grateful to Dr. Wagner B. De Almeida, Dr. Oliver Howarth, and Dr. David Lee Nelson for helpful discussions, comments, and suggestions.

REFERENCES

[1] Laure, C.J. Die primärstruktur des crotamins. *Hoppe-Seyler's Z. Physiol. Chem.*, **1975**, *356*, 213-215.

[2] Owby, C.L. Structure, function and biophysical aspects of the myotoxins from snake venoms. *J. Toxicol.*, **1998**, *17*, 213-238.

[3] Kerkis, A.; Kerkis, I.; Rádis-Baptista, G.; Oliveira, E.B.; Vianna-Morgante, A.M.; Pereira, L.V.; Yamane, T. Crotamine is a novel cell-penetrating protein from the venom of rattlesnake *Crotalus durissus terrificus*. *FASEB J.*, **2004**, *18*, 1407-1409.

[4] Vital-Brazil, O.; Fontana, M.D. Toxins as tools in the study of sodium channel distribution in the muscle fibre membrane. *Toxicon*, **1993**, *31*, 1085-1098.

[5] Matavel, A.C.S.; Ferreira-Alves, D.L.; Beirão, P.S.L.; Cruz, J.S. Tension generation and increase in voltage-activated Na^+ current by crotamine. *Eur. J. Pharmacol.*, **1998**, *348*, 167-173.

[6] Mancin, A.C.; Soares, A.M.; Andrião-Escarso, S.H.; Faça, V.M.; Greene, L.J.; Zucolotto, S.; Pelá, I.R.; Giglio, J.R. The analgesic activity of crotamine, a neurotoxin from *Crotalus durissus terrificus* (South American rattlesnake) venom: a biochemical and pharmacological study. *Toxicon*, **1998**, *36*, 1927-1937.

[7] Cameron, D.L.; Tu, A.T. Chemical and functional homology of myotoxin A from prairie rattlesnake venom and crotamine from South American rattlesnake venom. *Biochem. Biophys. Acta*, **1978**, *532*, 147-154.

[8] Fletcher, J.E.; Hubert, M.; Wieland, S.J.; Gong, Q.; Jiang, M. Similarities and differences in mechanisms of cardiotoxins, melittin and other myotoxins. *Toxicon*, **1996**, *34*, 1301-1311.

[9] Dos-Santos, M.C.; Morhy, L.; Ferreira, L.C.L.; Oliveira, E.B. Purification and properties of a crotamine analog from *Crotalus durissus ruruima* venom. *Toxicon*, **1993**, *31*, 166.

[10] Nicastro, G.; Franzoni, L.; Chiara, C.; Mancin, A.C.; Giglio, J.R.; Spisni, A. Solution structure of crotamine, a Na^+ channel affecting toxin from *Crotalus durissus terrificus* venom. *Eur. J. Biochem.*, **2003**, *270*, 1969-1979.

[11] Fadel, V.; Bettendorff, P.; Herrmann, T.; Azevedo, W.F.; Oliveira, E.B.; Yamane, T.; Würthrich, K. Automated NMR structure determination and disulfide bond identification of the myotoxin crotamine from *Crotalus durissus terrificus*. *Toxicon*, **2005**, *46*, 759-767.

[12] Siqueira, A.M.; Martins, N.F.; De-Lima, M.E.; Diniz, C.R.; Cartier, A.; Brown, D.; Maigret, B. A proposed 3D structure for crotamine base don homology building, molecular simulation and circular dichroism. *J. Mol. Graph. Model.*, **2002**, *20*, 389-398.

[13] Gaussian 2003, Revision B.04: Frisch, M.J.; Trucks, G.W.; Schlegel, H.B.; Scuseria, G.E.; Robb, M.A.; Cheeseman, J.R.; Montgomery, J.A., Jr.; Vreven, T.; Kudin, K.N.; Burant, J.C.; Millam, J.M.; Iyengar, S.S.; Tomasi, J.; Barone, V.; Mennucci, B.; Cossi, M.; Scalmani, G.; Rega, N.; Petersson, G.A.; Nakatsuji, H.; Hada, M.; Ehara, M.; Toyota, K.; Fukuda, R.; Hasegawa, J.; Ishida, M.; Nakajima, T.; Honda, Y.; Kitao, O.; Nakai, H.; Klene, M.; Li, X.; Knox, J.E.; Hratchian, H.P.; Cross, J.B.; Adamo, C.; Jaramillo, J.; Gomperts, R.; Stratmann, R.E.; Yazyev, O.; Austin, A.J.; Cammi, R.; Pomelli, C.; Ochterski, J.W.; Ayala, P.Y.; Morokuma, K.; Voth, G.A.; Salvador, P.; Dannenberg, J.J.; Zakrzewski, V.G.; Dapprich, S.; Daniels, A.D.; Strain, M.C.; Farkas, O.; Malick, D.K.; Rabuck, A.D.; Raghavachari, K.; Foresman, J.B.; Ortiz, J.V.; Cui, Q.; Baboul, A.G.; Clifford, S.; Cioslowski, J.; Stefanov, B.B.; Liu, G.; Liashenko, A.; Piskorz, P.; Komaromi, I.; Martin, R.L.; Fox, D.J.; Keith, T.; Al-Laham, M.A.; Peng, C.Y.; Nanayakkara, A.; Challacombe, M.; Gill, P.M.W.; Johnson, B.; Chen, W.; Wong, M.W.; Gonzalez, C.; Pople, J.A. Gaussian, Inc., Pittsburgh PA, **2003**.

[14] Dewar, M.J.S.; Zoebish, E.G.; Healy, E.F.; Stewart, J.J.P. Development and use of quantum mechanical molecular models. AM1: a new general purpose quantum mechanical model. *J. Am. Chem. Soc.*, **1985**, *107*, 3902-3909.

[15] Binkley, J.S.; Pople, J.A.; Hehre, W.J. Self-consistent molecular orbital methods. 21. Small split-valence basis sets for first-row elements. *J. Am. Chem. Soc.*, **1980**, *102*, 939-947.

[16] Hariharan, P.C.; Pople, J.A. Accuracy of ΔH equilibrium geometries by single determinant molecular-orbital theory. *Mol. Phys.*, **1974**, *27*, 209-214.

[17] Gordon, M.S. The isomers of silacyclopropane. *Chem. Phys. Lett.*, **1980**, *76*, 163-168.

[18] Parr, R.G.; Yang W. *Density Functional Theory of Atoms and Molecules*; Oxford: New York, **1989**.

[19] Becke, A.D. Density-functional hermochemistry. III. The role of exact exchange. *J. Chem. Phys.*, **1993**, *98*, 5648-5652.

[20] Stephens, P.J.; Devlin, F.J.; Chabalowski, C.F.; Frisch, M.J. Ab initio calculation of vibrational absorption and circular dichroism spectra using density-functinal force-fields. *J. Phys. Chem.*, **1994**, *99*, 1623-1631.

[21] Foresman, J.B.; Frisch *Æ. Exploring Chemistry with Electronic Structure Methods*; Gaussian, Inc.: Pittsburgh, **1996**.

[22] Ramachandran, K.I.; Deepa, G.; Namboori, K. *Computational Chemistry and Molecular Modeling – Principles and Applications*; Springer: Heidelberg, **2008**.

[23] Barone, V.; Cossi, M.; Tomasi, J. A new definition of cavities for the computation of solvation free energies by the polarizable continuum model. *J. Chem. Phys.*, **1997**, *107*, 3210-3221.

[24] Abreu, H.A.; Lago, I.A.S.; Souza, G.P.; Piló-Veloso, D.; Duarte, H.A.; Alcântara, A.F.C. Antioxidant activity of (+)-bergenin a phytoconstituent isolated from the bark of *Sacoglottis uchi* Huber (Humireaceae). *Org. Biomol. Chem.*, **2008**, *6*, 2713-2718.

[25] Alcântara, A.F.C.; Piló-Veloso, D.; Almeida, W.B.; Maltha, C.R.A.; Barbosa, L.C.A. Conformational analysis of 8-oxabicyclo[3.2.1]oct-6-en-3-one derivatives by NMR and theoretical calculations. *J. Mol. Struct.*, **2006**, *791*, 180-185.

[26] Vieira, F.T.; Lima, G.M.; Wardell, J.L.; Wardell, S.M.S.V.; Krambrock, K.; Alcântara, A.F.C. Synthesis and characterization of [chloro{2(1H)-pyridinethione-S}{tris(pyridin-2-ylthiolato)methyl-C,N,N0,N00]}nickel(II)], [Ni(TPTM)(SPyH)Cl]. *J. Organomet. Chem.*, **2008**, *693*, 1986-1990.

[27] Denadai, A.M.L.; Ianzer, D.; Alcântara, A.F.C.; Santoro, M.M.; Santos, C.F.F.; Lula, I.S.; Camargo, A.C.M.; Faljoni-Alario, A.; Santos, R.A.S.; Sinisterra, R.D. Novel pharmaceutical composition of bradykinin potentiating penta peptide with *β*-cyclodextrin: Physical–chemical characterization and anti-hypertensive evaluation. *Intern. J. Pharm.*, **2007**, *336*, 90-98.

[28] Munhoz, V.H.O.; Alcântara, A.F.C.; Piló-Veloso, D. Análise conformacional por cálculos teóricos da distinctina, peptídeo antimicrobiano isolado de anuros da espécie *Phyllomedusa distincta*. *Quim. Nova*, **2008**, *31*, 822-827.

[29] Careri, G. Cooperative charge fluctuations by migrating protons in globular proteins. *Prog. Biophys. Mol. Biol.*, **1998**, *70*, 223-249.

[30] Bourne, P.E.; Weissig, H. *Structural Bioinformatics*, Wiley-Liss: New Jersey, **2003**.

[31] Boni-Mitake, M.; Costa, H.; Spencer, P.J.; Vassilieff, V.S.; Rogero, J.R. Effects of ^{60}Co gamma radiation on crotamine. *Braz. J. Med. Biol. Res.*, **2001**, *34*, 1531-1538.

[32] Baker, B.; Tu, A.T.; Middlebrook, J.L. Binding of myotoxin A to cultured muscle cells. *Toxicon*, **1993**, *31*, 271-284.

[33] Beltran, J.R.; Mascarenhas, Y.P.; Craievich, A.F.; Laure, C.J. SAXS study of the snake toxin α-crotamine. *Eur. Biophys. J.*, **1990**, *17*, 325-329.

Received: July 27, 2009 Revised: August 06, 2010 Accepted: August 26, 2010